Published for SISSA by Springer

Received: October 24, 2019
Revised: February 26, 2020
Accepted: April 9, 2020
Published: April 28, 2020

JHEP04(2020)183

The Odderon in QCD with running coupling

Jochen Bartels,[a] **Carlos Contreras**[b] **and Gian Paolo Vacca**[c]

[a] *II. Institut für Theoretische Physik, Universität Hamburg, Luruper Chaussee 149, D-22761 Hamburg, Germany*
[b] *Departamento de Fisica, Universidad Tecnica Federico Santa Maria, Avda. España 1680, Casilla 110-V, Valparaiso, Chile*
[c] *INFN — Sezione di Bologna, DIFA, via Irnerio 46, I-40126 Bologna, Italy*

E-mail: jochen.bartels@desy.de, carlos.contreras@usm.cl, vacca@bo.infn.it

Abstract: Starting from the leading Odderon solution of the three gluon system in perturbative QCD we introduce, as a first step towards the transition to the non-perturbative region, an infrared cutoff and use the running QCD coupling constant. In our numerical analysis we find that the fixed cut solution with intercept one persists, hinting at a physical Odderon with intercept one and a small t-slope.

Keywords: Perturbative QCD, Resummation

ArXiv ePrint: 1910.04588

https://doi.org/10.1007/JHEP04(2020)183

Contents

JHEP04(2020)183

1 Introduction

Recently TOTEM [1–3] data have stimulated [4] a vivid discussion whether, in addition to the C-even Pomeron, also a C-odd Odderon exchange is needed to describe the data. After the proposal of Lukaszuk and Nicolescu [5] in 1973, it was the ISR data for $\frac{d\sigma}{dt}$ which indicated a difference between pp and $p\bar{p}$ and hence raised the quest for a C-odd exchange at high energies. A first connection with QCD was made by Donnachie and Landshoff [6] who introduced a three-gluon exchange as a model for the Odderon.

In the early 80's, soon after the discovery of the perturbative QCD Pomeron (BFKL) [7–10], which describes the composite state of two reggeized gluons it was realized that this picture can be generalized to composite states of three (and more) reggeized gluons, the so-called BKP states [11, 12]. A first solution of the three gluon problem was found by Janik and Wosiek [13] (JW) and its intercept was found to be $\alpha_O = 1 - 0.24717\frac{\alpha_s N_c}{\pi}$, which for a realistic $\alpha_s = 0.2$ yields $\alpha_O = 0.96$. In 1999 another solution was found by Bartels, Lipatov, and Vacca [14] (BLV) with intercept exactly at one, $\alpha_O = 1$, independent of the value of α_s. A remarkable feature of this solution of the three gluon composite state equation is that it coincides with the two gluon BFKL solution with conformal spin $n = 1$. A discussion of the relevance of the JW and the BLV solutions in phenomenology prior to LHC data can be found in [15, 16].

These perturbative results cannot directly be applied to soft hadron-hadron scattering. However, in recent years some progress has been made in analyzing the transition from the perturbative BFKL Pomeron to the soft Pomeron. Starting from the perturbative region and replacing the fixed coupling by the running coupling, first an infrared cutoff has to be introduced. These steps lead to important changes of the energy spectrum: for fixed coupling the BFKL Pomeron has a fixed (i.e. t-independent) cut in the ω plane (angular

momentum $j = \omega + 1$), starting at $\omega_{cut} = \frac{N_c \alpha_s}{\pi} 4 \ln 2$ and extending to $-\infty$. In the presence of an infrared cutoff and with running α_s the piece of the ω-cut between ω_{cut} and zero is replaced by an infinite sequence of discrete poles, which accumulate at zero. This picture has been verified in numerical studies, for several different versions of an infrared cutoff: in [17] an infrared cutoff has been introduced in such a way that the BFKL bootstrap property (related to s-channel unitarity) is preserved; in [18–20] boundary values of the BFKL amplitude are imposed at a fixed momentum scale k_0^2; in [21–23] a Higgs mass is introduced as an IR regulator, and in [24] a more sophisticated regulator is introduced which allows to embed the BFKL Pomeron into RG flow equations. Details of this discrete spectrum in the ω-plane of course depend upon the value of the cutoff scale and vary from one scheme to another, but the qualitative picture is the same in all schemes. Next, for this discrete part of the spectrum also the eigenfunctions have been studied [24]: most important, it has been found that only for the leading eigenvalue the wave function is centered in the 'soft' region of small transverse momenta, whereas for the nonleading eigenvalues the wave functions become 'hard', i.e. these Pomeron states are centered in the UV-region of large transverse momenta. Consequently, their couplings to hadron states are expected to be small. Finally, the t-slopes [24] of these discrete poles are largest for the leading eigenvalue, and go to zero for the nonleading poles. These findings suggest that these two steps — introduction of an infrared cutoff and of the running coupling — bring us substantially closer to the nonperturbative region, in particular the existence of a 'soft' Pomeron state with intercept above one. What remains is the 'unitarization' of this set of Pomeron states: this requires, in particular, the introduction of the triple Pomeron vertex. Work along this line is in progress.

Applying these findings to the three gluon problem of the Odderon, which for the BLV solution again reduces to a two gluon BFKL Pomeron problem with odd conformal spin ($n = 1$), it seems plausible to proceed in the same manner: introduce an infrared cutoff and the running coupling and then study the energy spectrum. As already stated before, the leading BLV Odderon solution without IR cutoff and with fixed coupling leads to a fixed (i.e. t-independent) cut in the ω plane, starting at $\omega = 0$ and extending to $-\infty$. In this paper we will investigate how this picture changes, once we introduce an IR cutoff and the running coupling. For simplicity we use the Higgs-mass regulator, and we use the numerical methods outlined in [24]. As the main result, we find that the spectrum remains unchanged, i.e. we still have a cut starting at $\omega = 0$. The wave functions are 'hard', i.e they have their main support in the region of large transverse momenta, and the t-slopes are small. An analysis of what happens to the other family of Odderon solutions (JW) with lower intercept is unfortunately much more involved, and it is extremely difficult to carry on employing a similar approach.

The paper will be organized as follows. In section 2 we review the BFKL kernel with Higgs mass regulator for $n = 1$ in the forward direction, and after introducing for the fixed coupling case the lattice approximation we present numerical results for the eigenvalue spectrum and for the eigenfunctions. This part is mainly meant to verify that our lattice approximation is consistent with our knowledge of the analytic BLV solution. In section 3 we turn to the running coupling case and compute eigenvalues, eigenfunctions and t-slopes. In a final section we summarize and discuss our results.

JHEP04(2020)183

2 The $n = 1$ BFKL kernel with a Higgs mass regulator

In this section we present the BFKL kernel with an infrared cutoff and specialize to the case of spin $n = 1$ which has been associated to a family of leading Odderon states. This general problem for the Pomeron channel has been addressed before in previous papers [24] and [21–23], which we partly follow.

In our previous paper [24] we have performed a numerical study of the BFKL kernel for the Pomeron case with two infrared regulators. In particular in our analysis we have considered both the Wilsonian optimized IR regulator in the exact functional renormalization group approach (this regulator was constructed in such a way that the BFKL Pomeron Green's function can be extracted from the flow induced by the exact renormalization group equation for the effective average action functional in the Multi Regge Kinematics (MRK)) and we have also carried out a numerical study of the BFKL Pomeron with a "gluon mass" regulator. In both cases we computed the energy eigenvalues (i.e. poles in the angular momentum plane), in particular intercepts and q^2 slopes of the Regge trajectory functions and eigenfunctions of the BFKL kernel. In our results for the Wilsonian regulator and the mass regulator, qualitatively, there are no differences and therefore the general behavior is apparently independent of the regulator.

In the following subsections we shall set up the spectral problem and perform a numerical analysis of the IR modified BFKL kernel for the fixed QCD coupling, introducing a simple mass regulator, limiting ourselves to the forward direction in order to study the Odderon eigenvalues (intercept) and eigenstates. In a second step, in the next section, we shall consider a running gauge coupling and compute also the $\mathbf{q}^2$-slope (known as t-slope) of the BLV Odderon of the trajectory function, which is defined as the first derivative with respect to $\mathbf{q}^2$. In the Pomeron case, we found a set of discrete spectrum so that one can make a link at large distances with the local Pomeron fields of a Reggeon Field Theory (RFT). Therefore we shall look for evidence of such a case for the Odderon. We remind that the properties of both Pomeron and Odderon as a RFT, including their universal properties, have been recently investigated using functional renormalization group methods in [25, 26]. The numerical analysis proceeds in two steps. First we shall study the eigenvalues and eigenfunctions of the BFKL Odderon equation with the mass regulator, then what is new in our analysis are the $\mathbf{q}^2$ slopes of the Odderon states. In a future paper we shall turn to the Wilsonian IR regulator and, again, compute those relevant properties.

2.1 The $n = 1$ BFKL equation

We begin with the Higgs mass regulated BFKL kernel with fixed coupling in the general non forward direction. Since the four momenta of the Green's function $\mathbf{q}_1, \mathbf{q}_2, \mathbf{q}'_1, \mathbf{q}'_2$ are not independent and the total transverse momentum $\mathbf{q} = \mathbf{q}_1 + \mathbf{q}_2 = \mathbf{q}'_1 + \mathbf{q}'_2$ exchanged in the t-channel is conserved, it is convenient to first introduce two relative momenta $\mathbf{k}$, $\mathbf{k}'$:

$$\mathbf{q}_1 = \frac{\mathbf{q}}{2} + \mathbf{k}, \;\; \mathbf{q}_2 = \frac{\mathbf{q}}{2} - \mathbf{k}, \;\; \mathbf{q}'_1 = \frac{\mathbf{q}}{2} + \mathbf{k}', \;\; \mathbf{q}'_2 = \frac{\mathbf{q}}{2} - \mathbf{k}' \,. \tag{2.1}$$

JHEP04(2020)183

The analytic expression of the symmetrized[1] BFKL kernels (the real part associated to gluon emission) has the form

$$\begin{aligned}\frac{2\pi}{\bar{\alpha}_s}K(\mathbf{q},\mathbf{k},\mathbf{k}') = &\sqrt{\frac{\mathbf{q}_1^2+m^2}{\mathbf{q}_2^2+m^2}}\frac{1}{(\mathbf{k}-\mathbf{k}')^2+m^2}\sqrt{\frac{\mathbf{q}_2'^2+m^2}{\mathbf{q}_1'^2+m^2}}\\ &+\sqrt{\frac{\mathbf{q}_2^2+m^2}{\mathbf{q}_1^2+m^2}}\frac{1}{(\mathbf{k}-\mathbf{k}')^2+m^2}\sqrt{\frac{\mathbf{q}_1'^2+m^2}{\mathbf{q}_2'^2+m^2}}\\ &-\frac{\mathbf{q}^2+\frac{N_c^2+1}{N_c^2}m^2}{\sqrt{(\mathbf{q}_1^2+m^2)(\mathbf{q}_2^2+m^2)(\mathbf{q}_1'^2+m^2)(\mathbf{q}_2'^2+m^2)}}\end{aligned} \tag{2.2}$$

where $\bar{\alpha}_s = \frac{N_c\alpha_s}{\pi}$, and the gluon trajectory function (virtual part of the BFKL kernel) has the form:

$$\begin{aligned}\omega_g(\mathbf{k}^2) &= -\frac{\bar{\alpha}_s}{4\pi}\int d^2k'\frac{\mathbf{k}^2+m^2}{(\mathbf{k}'^2+m^2)((\mathbf{k}-\mathbf{k}')^2+m^2)}\\ &= -\frac{\bar{\alpha}_s}{2\pi}\int d^2k'\frac{\mathbf{k}^2+m^2}{(\mathbf{k}'^2+m^2)(\mathbf{k}'^2+(\mathbf{k}-\mathbf{k}')^2+2m^2)}\,.\end{aligned} \tag{2.3}$$

The full BFKL kernel is then given by:

$$\tilde{K}(\mathbf{q},\mathbf{k},\mathbf{k}') = K(\mathbf{q},\mathbf{k},\mathbf{k}') + \delta^{(2)}(\mathbf{k}-\mathbf{k}')\left(\omega_g(\mathbf{q}_1^2)+\omega_g(\mathbf{q}_2^2)\right)\,. \tag{2.4}$$

We consider in this section the forward direction $\mathbf{q}^2 = 0$ where the kernel simplifies:

$$\frac{2\pi}{\bar{\alpha}_s}K^{(0)}(\mathbf{k},\mathbf{k}') = \frac{2}{(\mathbf{k}-\mathbf{k}')^2+m^2} - \frac{\frac{N_c^2+1}{N_c^2}m^2}{(\mathbf{k}^2+m^2)(\mathbf{k}'^2+m^2)} \tag{2.5}$$

and

$$\tilde{K}^{(0)}(\mathbf{k},\mathbf{k}') = K^{(0)}(\mathbf{k},\mathbf{k}') + 2\delta^{(2)}(\mathbf{k}-\mathbf{k}')\omega_g(\mathbf{k}^2)\,. \tag{2.6}$$

The eigenvalue equation takes the form:

$$\omega f_\omega(\mathbf{k}) = \frac{\bar{\alpha}_s}{2\pi}\int d^2\mathbf{k}'\tilde{K}^{(0)}(\mathbf{k},\mathbf{k}')f_\omega(\mathbf{k}')\,. \tag{2.7}$$

In this paper we are interested in eigenvalues and eigenfunctions with conformal spin 1:

$$f(\mathbf{k}) = e^{i\varphi}\tilde{f}(|\mathbf{k}|), \tag{2.8}$$

where φ is the azimutal angle of the vector $\mathbf{k}$.

In order to study the $\mathbf{q}^2$ dependence of the eigenvalues $\omega(\mathbf{q}^2)$, we have to leave the forward direction. As usual we limit ourselves to the linear approximation:[2]

$$\omega(\mathbf{q}^2) = \omega(0) + \alpha'\mathbf{q}^2 + \cdots\,, \tag{2.9}$$

[1] Symmetrization refers to the gluon propagator to the right and left of the BFKL kernel. After a similarity transformation one can have a symmetric operator and therefore a symmetric matrix after discretization. The scattering amplitudes are invariant under such a transformation if the impact factors are transformed accordingly.

[2] In a complete non forward analysis the full momentum $\mathbf{q}$ dependence would be a much harder problem to solve. Also the higher order depedence should be studied to infer the region of validity of the linear approximation.

JHEP04(2020)183

where $\omega(0)$ denotes the intercept and α' the slope (also: $\mathbf{q}^2$ slope). For our numerical analysis of the eigenvalue equation (forward direction) it will be convenient to combine terms which contain the potentially singular denominator $1/(\mathbf{k}-\mathbf{k}')^2$ and to rewrite the eigenvalue equation in the following form [24]:

$$\omega f(\mathbf{k}) = \frac{\bar{\alpha}_s}{2\pi}\int d^2k' \left[\frac{2f(\mathbf{k}')(\mathbf{k}'^2+m^2)-2f(\mathbf{k})(\mathbf{k}^2+m^2)}{(\mathbf{k}'^2+m^2)((\mathbf{k}-\mathbf{k}')^2+m^2)} - \frac{\frac{N_c^2+1}{N_c^2}m^2}{(\mathbf{k}^2+m^2)(\mathbf{k}'^2+m^2)}f(\mathbf{k}')\right]$$
$$+\frac{\bar{\alpha}_s}{2\pi}\int d^2k' \frac{2f(\mathbf{k})(\mathbf{k}^2+m^2)}{(\mathbf{k}'^2+m^2)(\mathbf{k}'^2+(\mathbf{k}-\mathbf{k}')^2+2m^2)}. \tag{2.10}$$

This form has an integrand behaving manifestly better at large momenta $|\mathbf{k}| \sim |\mathbf{k}'| \to \infty$. We are interested in eigenfunctions of the form (2.8) and consider the following form of the eigenvalue equation:

$$\omega\tilde{f}(|\mathbf{k}|) = \frac{\bar{\alpha}_s}{2\pi}\int d^2k' \left[\frac{2\tilde{f}(|\mathbf{k}'|)e^{i(\varphi'-\varphi)}(\mathbf{k}'^2+m^2)-2\tilde{f}(|\mathbf{k}|)|(\mathbf{k}^2+m^2)}{(\mathbf{k}'^2+m^2)((\mathbf{k}-\mathbf{k}')^2+m^2)}\right]$$
$$+\frac{\bar{\alpha}_s}{2\pi}\int d^2k' \frac{2\tilde{f}(|\mathbf{k}|)(\mathbf{k}^2+m^2)}{(\mathbf{k}'^2+m^2)(\mathbf{k}'^2+(\mathbf{k}-\mathbf{k}')^2+2m^2)}. \tag{2.11}$$

Here φ and φ' denote the azimutal angles of the vectors $\mathbf{k}$ and $\mathbf{k}'$, respectively. We also introduce their modulus $k = |\mathbf{k}|$ and $k' = |\mathbf{k}'|$. The angular integrations can be done by using the formulae

$$\frac{1}{2\pi}\int_0^{2\pi} d\varphi \frac{1}{a+b\cos\varphi} = \frac{1}{\sqrt{a^2-b^2}}, \tag{2.12}$$

and

$$\frac{1}{2\pi}\int_0^{2\pi} d\varphi \frac{e^{i\varphi}}{a+b\cos\varphi} = \frac{1}{2\pi}\int_0^{2\pi} d\varphi \frac{\cos\varphi}{a+b\cos\varphi} = \frac{-b}{a+\sqrt{a^2-b^2}}\frac{1}{\sqrt{a^2-b^2}}, \tag{2.13}$$

where

$$a = k^2+k'^2+m^2,\ b = -2kk'. \tag{2.14}$$

Introducing the shorthand notations

$$D = k^2+m^2,\ D' = k'^2+m^2 \tag{2.15}$$

and

$$S_0 = \sqrt{(k^2-k'^2)^2+2m^2(k^2+k'^2)+m^4},$$
$$S_1 = k^2+k'^2+m^2+S_0$$
$$S_2 = \sqrt{(k^2-k'^2)^2+2(k'^2+2m^2)(k^2+k'^2)+(k'^2+2m^2)^2} \tag{2.16}$$

the eigenvalue equation in the forward direction can be written as:

$$\omega f(k) = \bar{\alpha}_s\int_0^\infty dk'^2\left[\frac{2kk'}{S_1}\frac{D'}{D'S_0}f(k') - \frac{D}{D'S_0}f(k)\right] + \bar{\alpha}_s\int_0^\infty dk'^2\frac{D}{D'S_2}. \tag{2.17}$$

In the following we present our numerical results of the Odderon eigenvalues and the wave functions. The latter will be written as functions of the dimensionless variable k/m and will be denoted as $f_n(k/m)$ with corresponding eigenvalue ω_n.

JHEP04(2020)183

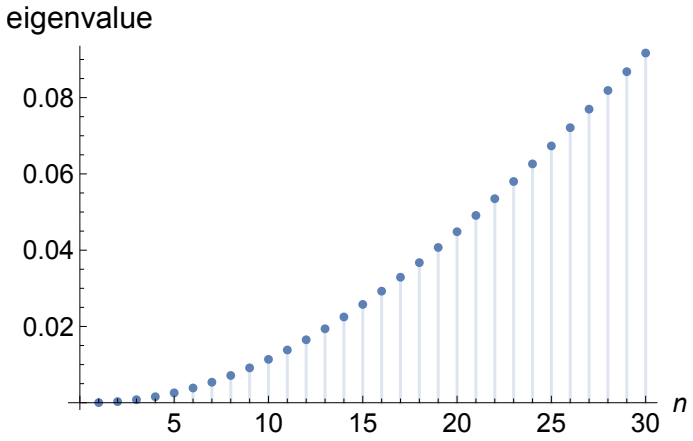

Figure 1. The first 30 eigenvalues of the Odderon with fixed coupling.

2.2 Numerical results for eigenvalues and eigenfunctions for fixed coupling

The numerical analysis of the eigenvalue equation (2.17) is done in the same way as described in [24]: for the integration over k'^2 we introduce a lattice. First we change to logarithmic variables $t' = \ln \frac{k'^2}{m^2}$ with $dk'^2 = dt' k'^2$ and then introduce a lattice in the new variables t'. For fixed coupling and zero infrared mass regulator we know that solutions have a scale invariant power-like behavior so that it is natural to expect that the best sampling is linear in the logarithmic variable. Indeed we find that this is a far more efficient method also when scale invariance is slightly broken, after comparing to alternative numerical methods employing more sophisticated grids. We use for the momenta the unit $m = 0.54\,\mathrm{GeV}$ which corresponds to our IR mass regulator. We shall come back to this at the beginning of section 3. Introducing the limits $k^2_{\min}/m^2 = 10^{-40}, t_{\min} = \ln \frac{k^2_{\min}}{m^2}$ and $k^2_{\max}/m^2 = 10^{80}, t_{\max} = \ln \frac{k^2_{\max}}{m^2}$ and dividing the interval $\left[t_{\min}, t_{\max}\right]$ into $N_{\mathrm{step}} = 600$ equal steps, we define the lattice points

$$t_i = t_{\min} + i \frac{t_{\max} - t_{\min}}{N_{\mathrm{step}}}, \;\; k_i^2 = m^2 e^{t_i}, \;\; i = 0, \ldots, N_{\mathrm{step}} \tag{2.18}$$

and arrive at the discrete vector $f_i = f(k_i)$ and the discrete matrix $K_{ij} = \tilde{K}^{(0)}(k_i, k_j)$, associated to the forward discretized kernel.

For the eigenvalues it is convenient to introduce

$$E_n = -\omega_n \,. \tag{2.19}$$

We find discrete positive "energy" eigenvalues E_n, the smallest one being very close to zero (for the energy dependence of the scattering amplitude this smallest value is the leading one). The first three values are:

$$E_1 = 0.000032, \quad E_2 = 0.000289, \quad E_3 = 0.000802. \tag{2.20}$$

In figure 1 we present the first 30 eigenvalues of the Odderon with fixed coupling constant.

We interpret these eigenvalues as being the lattice approximation of a cut in the positive energy plane, starting at zero. Indeed at fixed coupling this is known to be the case for

JHEP04(2020)183

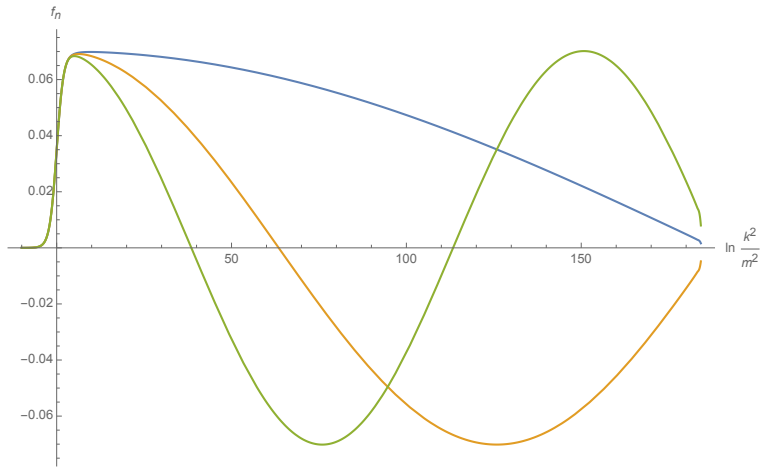

Figure 2. The first three wavefunctions for fixed coupling, as a function of $\ln \frac{k^2}{m^2}$. States with $n = 1, 2, 3$ correspond to color blue, orange and green, respectively.

the analytical solutions existing in the absence of the IR mass regulator and it has been observed also in another analysis [31]. As to the eigenfunctions, we find that they oscillate: the leading one has one maximum, the second one has one zero and has two extrema etc. The oscillations extend over the full lattice, to be more precise the full region $\mathbf{k}^2 > m^2$, and for larger values of k^2 the role of the mass IR cutoff is being felt less and less. As a consequnce the scaling behavior of the wavefunction towards the UV is fulfilled better and better. In figure 2 we show the first three eigenfunctions.

To make the support of the wavefunctions a bit more quantitative, we define the logarithmic radius

$$< \ln \frac{k^2}{m^2} >= \frac{\int dk^2 |f_n(\frac{k}{m})|^2 \ln \frac{k^2}{m^2}}{\int dk^2 |f_n(\frac{k}{m})|^2} \,, \tag{2.21}$$

where momenta are measured in units of $m = 0.54\,\text{GeV}$ chosen as a representative non perturbative QCD scale. By exponentiating this logarithmic radius we translate these logarithmic radii to the linear scale. For the lowest eigenvalues we find for the logarithmic radii

$$\begin{aligned} < \ln \frac{k^2}{m^2} >_1 &= 56.75 \\ < \ln \frac{k^2}{m^2} >_2 &= 90.39 \\ < \ln \frac{k^2}{m^2} >_3 &= 93.04 \,, \end{aligned} \tag{2.22}$$

and for the linear radii

$$\begin{aligned} r_1 &= 1.14 \times 10^{12}\,\text{GeV} \\ r_2 &= 2.30 \times 10^{19}\,\text{GeV} \\ r_3 &= 8.62 \times 10^{19}\,\text{GeV}. \end{aligned} \tag{2.23}$$

More general, in figure 3 we show, for the first 20 eigenfunctions, the logarithmic and linear radii.

JHEP04(2020)183

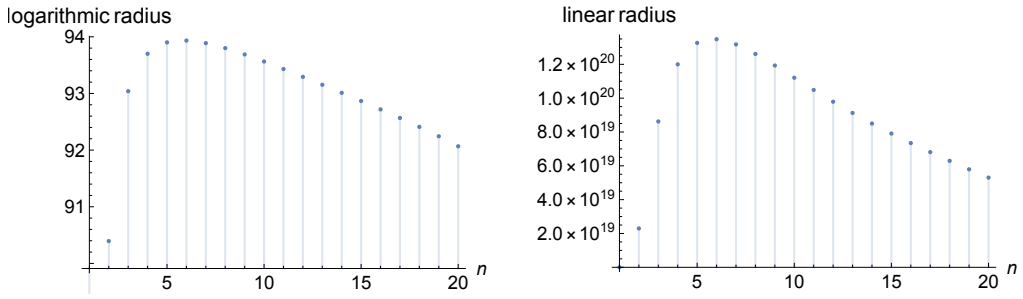

Figure 3. Logarithmic (left) and linear (right) radii for the first 20 eigenfunctions.

3 The Odderon solutions for the running coupling constant

3.1 Introducing the running coupling and leaving the forward direction

Let us now turn to the case of the running coupling. We follow the discussion of our previous paper [24]. As a first step we perform an RG improvement and simply replace the fixed coupling α_s by

$$\alpha_s(\mathbf{q}^2) = \frac{3.41}{\beta_0 \ln \frac{\mathbf{q}^2+R_0^2}{\Lambda^2_{\rm QCD}}} \tag{3.1}$$

and define

$$\bar{\alpha}_s(\mathbf{q}^2) = \alpha_s(\mathbf{q}^2)\frac{N_c}{\pi} \tag{3.2}$$

with $\beta_0 = (11N_c - 2N_f)/12$, $N_f = 3$. Its normalization is chosen to match the measured value at the Z mass scale. R_0 defines the scale below which the running coupling is 'frozen'. Both q^2 and R_0^2 appear in units of $\Lambda^2_{\rm QCD}$, and R_0^2 has to be well above $\Lambda^2_{\rm QCD} = 0.15^2\,{\rm GeV}^2$. More accurate models allowing for different number of flavors can be easily considered. In our numerical computations with our mass regulator we actually find it convenient to follow the conventions used in [21, 23]: we define momenta and R_0 in units of the regulator mass $m = 0.54\,{\rm GeV}$. This leads to the modification of (3.1):

$$\alpha_s(\mathbf{q}^2) = \frac{3.41}{\beta_0\left[\ln \frac{\mathbf{q}^2+R_0^2}{m^2} + \ln \frac{m^2}{\Lambda^2_{\rm QCD}}\right]} \tag{3.3}$$

with $R_0 = 1$.

The inclusion of the QCD running coupling effects in the Regge limit is a delicate issue when considering a full resummation. Strictly speaking this effect goes beyond the Leading Log contribution in the region of multiregge kinematics (MRK), where by definition any real gluon is emitted far in rapidity from all the others, since one has to take into account emissions of at least two real gluons close in rapidity, which start from the region called quasi MRK and are suppressed by a $\log s$ with respect to the leading ones. It is also well known that the BFKL Pomeron in NLL accuracy has a spectrum which must be cured in the collinear region with subleading terms (which do not alter the NLL accuracy in the Regge limit), and several approaches have been proposed [27, 28]. The same situation can be observed for the QCD perturbative Odderon, for which the kernel is also known to the

JHEP04(2020)183

NLL accuracy [29] and a solution with intercept at one is also expected [30], at least in the large N_c limit.

There is, however, a consensus that a good understanding of the pure running coupling effects can be nevertheless obtained by directly improving the picture obtained from the leading logarithmic approximation, that is by simply replacing the fixed coupling by a running coupling, even if this approach is not unique.[3] We shall take this attitude and consider in our calculationthe following prescription [24]:

(i) in the trajectory function $\omega_g(\mathbf{q}_i^2)$ we simply make the replacement

$$\alpha_s \to \alpha_s(\mathbf{q}_i^2)\,. \tag{3.4}$$

(ii) in the real kernel $K_{\rm BFKL}(\mathbf{q},\mathbf{q}')$ in the forward direction one makes the following substitution

$$\alpha_s \to \sqrt{\alpha_s(\mathbf{q}^2)\alpha_s(\mathbf{q}'^2)}. \tag{3.5}$$

(iii) In the non-forward direction the kernel $K_{\rm BFKL}(\mathbf{q}_1,\mathbf{q}_2;\mathbf{q}_1',\mathbf{q}_2') = \tilde{K}(\mathbf{q},\mathbf{k},\mathbf{k}')$ is modified according to

$$\alpha_s \to \left(\alpha_s(\mathbf{q}_1^2)\alpha_s(\mathbf{q}_2^2)\alpha_s(\mathbf{q}_1'^2)\alpha_s(\mathbf{q}_2'^2)\right)^{1/4}. \tag{3.6}$$

As discussed before, we will consider this prescription as a first approximate attempt to include the running coupling and for the forward direction the eigenvalue equations will be modified in the following way:

$$\alpha_s(\mathbf{k}^2)K^{(0)}(\mathbf{k},\mathbf{k}') \to \sqrt{\alpha_s(\mathbf{k}^2)}K^{(0)}(\mathbf{k},\mathbf{k}')\sqrt{\alpha_s(\mathbf{k}'^2)}, \tag{3.7}$$

and the trajectory functions will be simply multiplied by $\alpha_s(\mathbf{k}^2)$.

Finally, for the t-slopes we have to leave the forward direction. In addition to the $\mathbf{q}^2$ expansions of the kernel and of the trajectory function described in section 7.2 of [24], we also need the expansion of the running couplings in (3.4) and (3.6). As we will see, in the computation of several expressions one has to plug in expansions where also terms linear in $\mathbf{q}$ are kept (see (3.15) and (3.16) below).

Next let us take a closer look at the dependence of the kernel on the momentum transfer $\mathbf{q}^2$. Again we start from [24], section 7.2. The $\mathbf{q}^2$ slopes of the eigenvalues are obtained from

$$\omega_n(\mathbf{q}^2) = \omega_n^{(0)} + \mathbf{q}^2 \frac{\int d^2\mathbf{k}\int d^2\mathbf{k}' f_n(\frac{k'}{m})\left[K^{(1)}(\mathbf{k},\mathbf{k}') + 2\delta^{(2)}(\mathbf{k}-\mathbf{k}')\omega_g^{(1)}(\mathbf{k}^2)\right] f_n(\frac{k}{m})}{\int d^2\mathbf{k}|f_n(\frac{k}{m})|^2}\,, \tag{3.8}$$

where $\omega_n^{(0)}$ are the eigenvalues of the forward kernel $K^{(0)}$, $f_n(k/m)$ the corresponding Odderon eigenfunctions, and $K^{(1)}$, $\omega^{(1)}$ the corrections of the order $\mathbf{q}^2$ to the forward BFKL kernel and the gluon trajectory, resp.

[3] Another possible approach preserving the bootstrap property as in [17] is considered in another analysis elsewhere [31].

JHEP04(2020)183

In order to find $K^{(1)}(\mathbf{k},\mathbf{k}')$ we expand the kernel in the small $\mathbf{q}^2$ region to first order in $\mathbf{q}^2$:

$$K(\mathbf{q},\mathbf{k},\mathbf{k}') = K^{(0)}(\mathbf{k},\mathbf{k}') + \mathbf{q}^2 K^{(1)}(\mathbf{k},\mathbf{k}'). \tag{3.9}$$

With the shorthand notations

$$D = k^2+m^2,\ D' = k'^2+m^2,\ D_0 = (\mathbf{k}-\mathbf{k}')^2+m^2 \tag{3.10}$$

we find:

$$\begin{aligned} K(\mathbf{q},\mathbf{k},\mathbf{k}') = \frac{\bar{\alpha}_s}{2\pi}\Bigg[&\frac{2}{D_0}\left(1-\frac{(2\mathbf{qk})(2\mathbf{qk}')}{4DD'}+\frac{(2\mathbf{qk})^2}{8D^2}+\frac{(2\mathbf{qk}')^2}{8D'^2}\right) \\ &-\frac{m^2\frac{N_c^2+1}{N_c^2}}{DD'}\left(1+\frac{1}{2}\left(\frac{\mathbf{qk}}{D}\right)^2+\frac{1}{2}\left(\frac{\mathbf{qk}'}{D'}\right)^2-\frac{\mathbf{q}^2}{4}\left(\frac{1}{D}+\frac{1}{D'}\right)\right)-\mathbf{q}^2\frac{1}{DD'}\Bigg]. \end{aligned} \tag{3.11}$$

Note that there are no terms of the order $\mathbf{q}$.

For the integration over the azimuthal angles in (3.8) we have to observe the angular dependence of the wave functions which leads to the additional factor

$$e^{i(\varphi-\varphi')}, \tag{3.12}$$

where φ and φ' denote the angle of the vectors $\mathbf{k}$ and $\mathbf{k}'$, resp. We immediately see that for the terms in the second line of (3.11) the angular integrations give zero. In the first line we use

$$\frac{1}{(2\pi)^2}\int_0^{2\pi}d\varphi\int_0^{2\pi}d\varphi' e^{i(\varphi-\varphi')}\frac{(2\mathbf{qk})(2\mathbf{qk}')}{(\mathbf{k}-\mathbf{k}')^2+m^2} = 2q^2kk'\frac{k^2+k'^2+m^2}{S_0S_1} \tag{3.13}$$

and

$$\frac{1}{(2\pi)^2}\int_0^{2\pi}d\varphi\int_0^{2\pi}d\varphi' e^{i(\varphi-\varphi')}\frac{(2\mathbf{qk})^2}{(\mathbf{k}-\mathbf{k}')^2+m^2} = 2q^2k^2\frac{2kk'}{S_0S_1}.$$

With these expressions we find:

$$\frac{1}{2\pi}\int_0^{2\pi}d\varphi\int_0^{2\pi}d\varphi' e^{i(\varphi-\varphi')}K^{(1)}(\mathbf{k},\mathbf{k}') = \bar{\alpha}_s\frac{2kk'}{S_1}\frac{1}{S_0DD'}\left(-\frac{m^2}{2}\right)\left[1+\frac{(k^2-k'^2)^2}{DD'}\right]. \tag{3.14}$$

For the $\mathbf{q}^2$-expansion of the trajectory function we have the same expressions as for the Pomeron case, since the delta functions $\delta^{(2)}(\mathbf{k}-\mathbf{k}')$ lead to $e^{i(\varphi-\varphi')}\to 1$. Following [24] we define

$$\omega_g\left(\left(\frac{\mathbf{q}}{2}+\mathbf{k}\right)^2\right) = \omega_g(\mathbf{k}^2)+\omega^{(1/2)}+\mathbf{q}^2\omega^{(1)}(\mathbf{k}^2) \tag{3.15}$$

and

$$\alpha_s\left(\left(\frac{\mathbf{q}}{2}+\mathbf{k}\right)^2\right) = \alpha_s(\mathbf{k}^2)\left[1+\alpha^{(1/2)}+\mathbf{q}^2\alpha^{(1)}(\mathbf{k}^2)\right], \tag{3.16}$$

where $\omega^{(1/2)}$ and $\alpha^{(1/2)}$ are of the order $\mathcal{O}(\mathbf{q})$. The RG improvement of the trajectory therefore leads the product of such expressions which should be azimutally averaged

$$\begin{aligned} &\langle\left[1+\alpha^{(1/2)}+\mathbf{q}^2\alpha^{(1)}(k^2)\right]\left[\omega_g(\mathbf{k}^2)+\omega^{(1/2)}+\mathbf{q}^2\omega^{(1)}(k^2)\right]\rangle \\ &\quad = \omega_g(\mathbf{k}^2)+\langle\alpha^{(1/2)}\omega^{(1/2)}\rangle+\mathbf{q}^2\alpha^{(1)}(\mathbf{k}^2)\omega_g(\mathbf{k}^2)+\mathbf{q}^2\omega^{(1)}(\mathbf{k}^2). \end{aligned} \tag{3.17}$$

JHEP04(2020)183

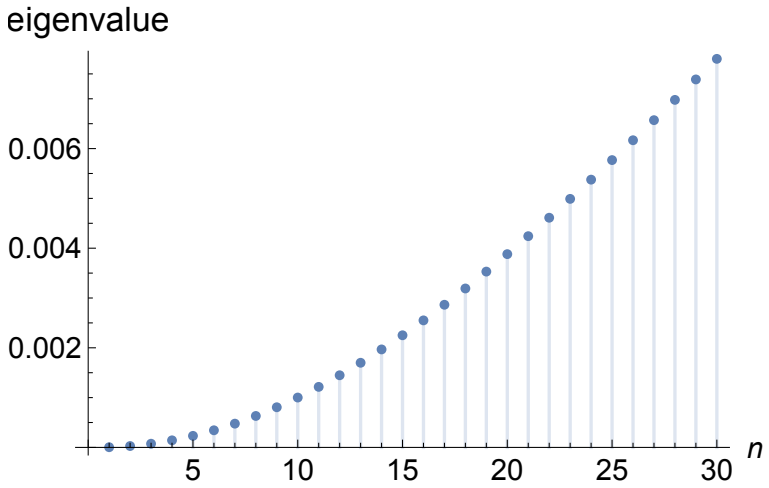

Figure 4. The first 30 eigenvalues.

The expressions for $\langle \alpha^{(1/2)} \omega^{(1/2)} \rangle$ and $\alpha^{(1)}(\mathbf{k}^2)$ can be found in eqs. (7.44) and (7.39) of [24] respectively. Moreover using also the expansion

$$\left(\alpha_s(\mathbf{q}_1^2)\alpha_s(\mathbf{q}_2^2)\alpha_s(\mathbf{q}_1'^2)\alpha_s(\mathbf{q}_2'^2)\right)^{\frac{1}{4}} = \sqrt{\alpha(\mathbf{k}^2)\alpha(\mathbf{k}'^2)}\left[1 + \mathbf{q}^2 \frac{\tilde{\alpha}(\mathbf{k}^2) + \tilde{\alpha}(\mathbf{k}'^2)}{2}\right], \tag{3.18}$$

where $\tilde{\alpha}(\mathbf{q}^2)$ can be found in eq. (7.41) of ref. [24] one has all the ingredients to compute the final result for the $\mathbf{q}^2$ part of eq. (3.11):

$$\begin{aligned}&\sqrt{\alpha(\mathbf{k}^2)\alpha(\mathbf{k}'^2)}K^{(1)}(\mathbf{k},\mathbf{k}') + 2\delta^{(2)}(\mathbf{k}-\mathbf{k}')\omega^{(1)}(\mathbf{k}^2) + 2\delta^{(2)}(\mathbf{k}-\mathbf{k}') < \alpha^{(1/2)}\omega^{(1/2)} > \\ &+ \left[\sqrt{\alpha(\mathbf{k}^2)\alpha(\mathbf{k}'^2)}K^{(0)}(\mathbf{k},\mathbf{k}') + 2\delta^{(2)}(\mathbf{k}-\mathbf{k}')\omega_g(\mathbf{k}^2)\right]\frac{\tilde{\alpha}(\mathbf{k}^2) + \tilde{\alpha}(\mathbf{k}'^2)}{2},\end{aligned} \tag{3.19}$$

from which we can obtain, for each eigenstate, the $\mathbf{q}^2$-slope. With these approximation we are now ready to present numerical results for the eigenvalues and for the slopes.

3.2 Numerical results

We begin with the eigenvalues. Again we introduce the energies $E_n = -\omega_n$ and find a sequence of positive eigenvalues starting at

$$E_1 = 4 \times 10^{-6}, \quad E_2 = 28 \times 10^{-6}, \quad E_3 = 74 \times 10^{-6}, \tag{3.20}$$

which we interpret as approximating a cut in the positive energy plane starting at zero. The first eigenvalues are shown in figure 4. The curve in figure 4 keeps the shape of figure 1 and is only shifted a little bit.

For the eigenfunctions we find that they again oscillate with same behaviour, extending over the full lattice region $\mathbf{k}^2 > m^2$.

The effect of the running coupling constant is mainly to smoothen the behaviour of the wave function, as one can see from the figure 2 and figure 5 and to shift the center of them

JHEP04(2020)183

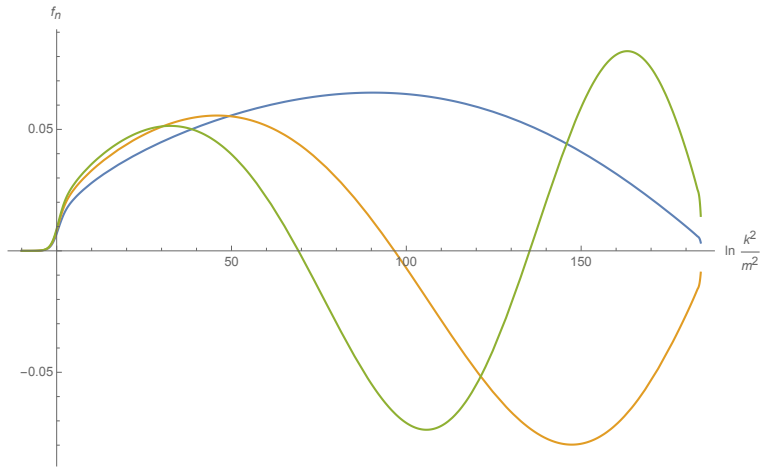

Figure 5. The first three wavefunctions as a function of $\ln \frac{k^2}{m^2}$ for the running coupling constant. States with $n = 1, 2, 3$ correspond to color blue, orange and green, respectively.

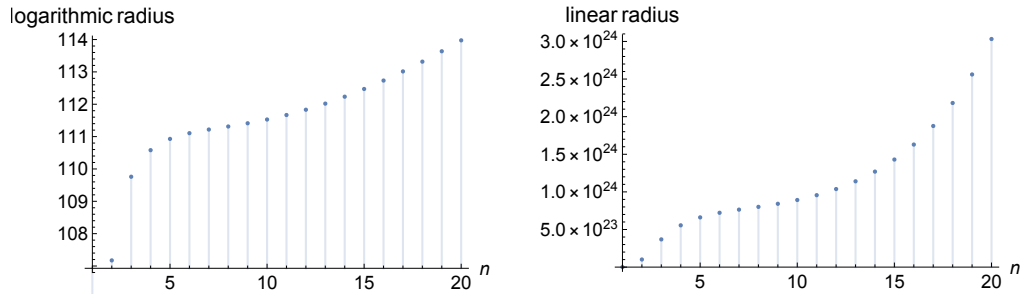

Figure 6. logarithmic (left) and linear (right) radii for the first 20 eigenfunctions for the running coupling.

to the right. For example, for the leading eigenvalue, the single node has its center (in the logarithmic scale) at approximately 88, compared with 57 for the fixed coupling case:

$$\begin{aligned} &< \ln \frac{k^2}{m^2} >_1 = 87.97 \\ &< \ln \frac{k^2}{m^2} >_2 = 107.26 \\ &< \ln \frac{k^2}{m^2} >_3 = 109.86\,, \end{aligned} \tag{3.21}$$

which translates into the linear radii

$$\begin{aligned} r_1 &= 6.83 \times 10^{18}\,\text{GeV} \\ r_2 &= 1.06 \times 10^{23}\,\text{GeV} \\ r_3 &= 3.89 \times 10^{23}\,\text{GeV}. \end{aligned} \tag{3.22}$$

More in general this is illustrated in figure 6.

JHEP04(2020)183

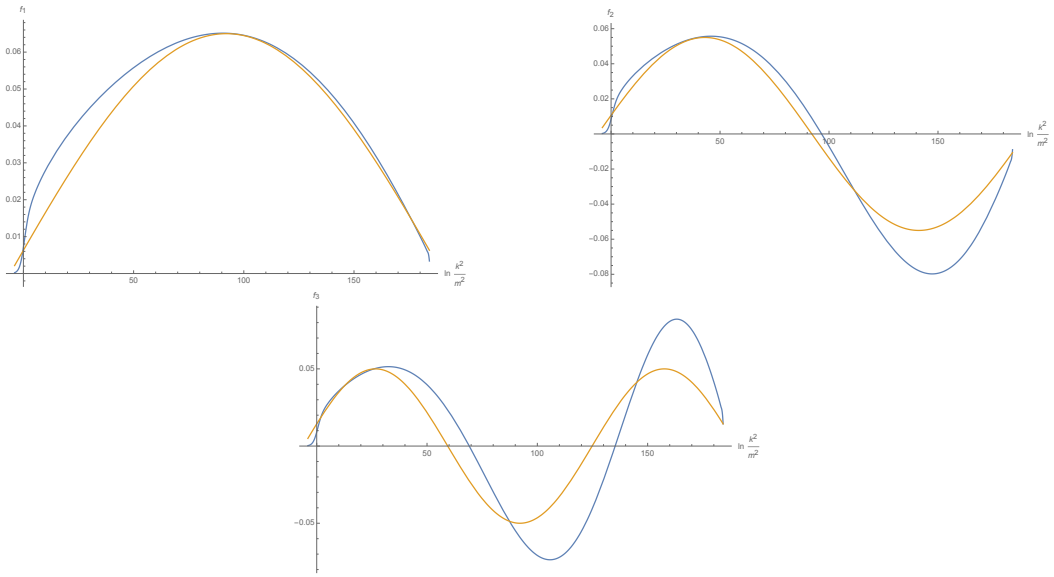

Figure 7. Comparison of the wave functions f_1, f_2 and f_3 (with the mass regulator) and running coupling constant (blue curve) versus pure oscillatory functions (orange curve) of eq. (3.25).

It may be useful to remember that for the massless case the BFKL eigenfunctions in the forward direction (for the symmetrized BFKL kernel) are given by

$$f(\mathbf{k}) \sim (k^2)^{-1/2-i\nu} e^{in\varphi}. \tag{3.23}$$

Near the beginning of the cut at $\omega = 0$ we have $\nu = 0$. Our lattice eigenfunctions have to be compared with $kf(\mathbf{k})$: our leading eigenfunctions should therefore be seen as the lattice approximation of

$$kf(\mathbf{k}) \sim (k^2)^{-i\nu}\ e^{i\varphi}. \tag{3.24}$$

Since we are introducing a mass as regulator of the infrared region, we expect that the wave function is suppressed in the region $k^2 < m^2$, and the form $(k^2)^{-i\nu}$ is valid only for larger values of k^2. Putting $t = \ln \frac{k^2}{m^2}$, we find that the wave function can be described approximately by

$$f_n(\frac{k}{m}) \sim \sin \nu_n (t - t^*) \quad , \quad \text{for } t > t^*(m)\,, \tag{3.25}$$

where t^* is a suitable parameter. For the first and second eigenfunctions we find that the behaviour is well described by $0.065 \sin \nu_1 (t - t^*)$ with $\nu_1 = \frac{\pi}{(t_{\max} - t^*)} = 0.016$, and by $0.055 \sin \nu_2 (t - t^*)$ with $\nu_2 = 2\nu_1$, respectively. In figure 7 one can see the behavior for leading wavefunction obtained with our mass regulator compared with the oscillatory behaviour of the massless case of the BFKL functions.

Finally, in figure 8 we show the behavior of the slopes from our numerical calculation. One can observe that the slope increases with n but still remain smaller than a few

JHEP04(2020)183

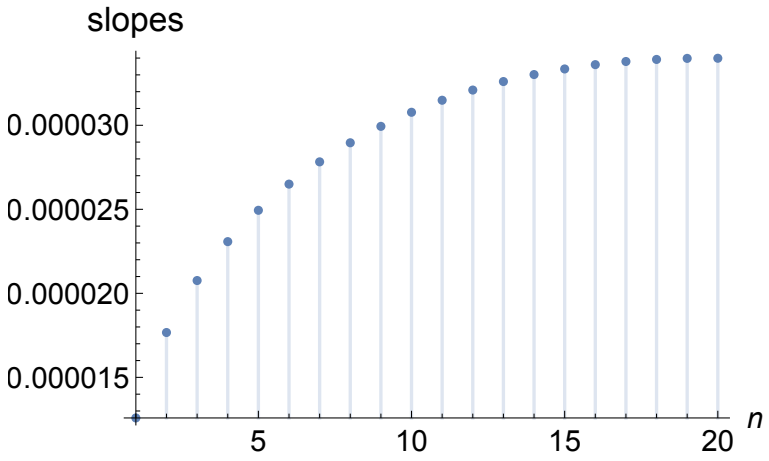

Figure 8. $\mathbf{q}^2$-slopes of the trajectory functions of the first 20 Odderon eigenstates.

times 10^{-5}. For the leading eigenvalues we find

$$\begin{aligned} E_1 &= 3.9 \times 10^{-6}, \qquad \alpha_1' = 1.26 \times 10^{-5} \\ E_2 &= 2.8 \times 10^{-5}, \qquad \alpha_2' = 1.77 \times 10^{-5} \\ E_3 &= 7.4 \times 10^{-5}, \qquad \alpha_3' = 2.08 \times 10^{-5}. \end{aligned} \tag{3.26}$$

3.3 Dependence on the lattice size

To further support our interpretation as a (fixed) cut in the energy plane, we note the following. In a continuum formulation of the BFKL eigenvalue equation, we expect the leading eigenvalue at exactly zero. For our finite lattice the leading eigenvalue turns out to be small and positive but nonzero, and for increasing lattice it should go to zero. Indeed, for the much larger lattices with $(e^{t_{\min}}, e^{t_{\max}}) = (10^{-40}, 10^{80})$, $(10^{-40}, 10^{100})$, $(10^{-40}, 10^{160})$ (keeping $N_{\text{step}} = 600$ fixed), one can see the decrease with increasing lattice size:

$$\begin{aligned} &E_1 = 3.9 \times 10^{-6}, \quad E_1 = 2.0 \times 10^{-6}, \quad E_1 = 4.7 \times 10^{-7}, \\ &E_2 = 2.8 \times 10^{-5}, \quad E_2 = 1.5 \times 10^{-5}, \quad E_2 = 3.6 \times 10^{-6}. \end{aligned} \tag{3.27}$$

More general, in figure 9 we show how all the eigenvalues decrease as we increase the upper limit $t_{\max}$.

Simultaneous variation of the upper and lower limit lead to a further decrease of the eigenvalues, e.g. for $N_{\text{step}} = 600$ and $(e^{t_{\min}}, e^{t_{\max}}) = (10^{-100}, 10^{160})$

$$E_1 = -3.38 \times 10^{-9}, E_2 = 3.11 \times 10^{-6}. \tag{3.28}$$

Finally, for comparison we also vary $N_{\text{step}} = 600, 1000$ and 1400, keeping the lattice size constant $(e^{t_{\min}}, e^{t_{\max}}) = (10^{-40}, 10^{80})$:

$$E_1 = 3.909 \times 10^{-6}, \; E_1 = 3.921 \times 10^{-6}, \; E_1 = 3.926 \times 10^{-6}\,. \tag{3.29}$$

This indicates that the numerical results are much less sensitive to N_{step}.

JHEP04(2020)183

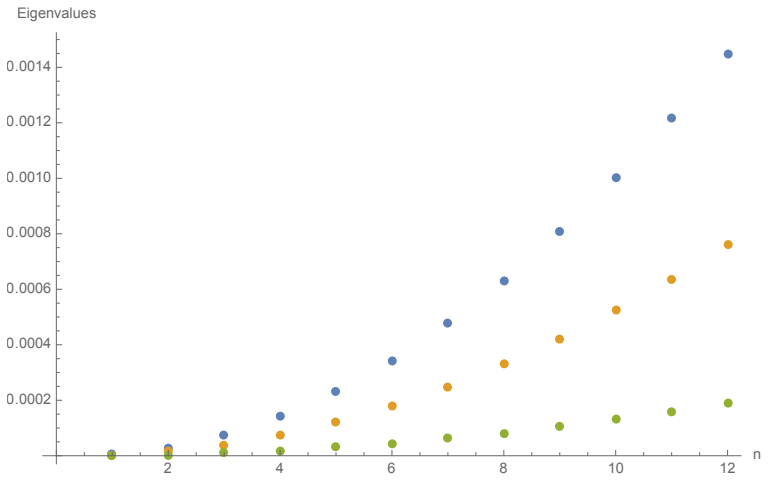

Figure 9. Behavior of the first twelve eigenvalues when we increase the upper limit of the lattice: $e^{t_{\max}} = 10^{80}, 10^{100}, 10^{160}$, represented in colors blue, orange and green respectively.

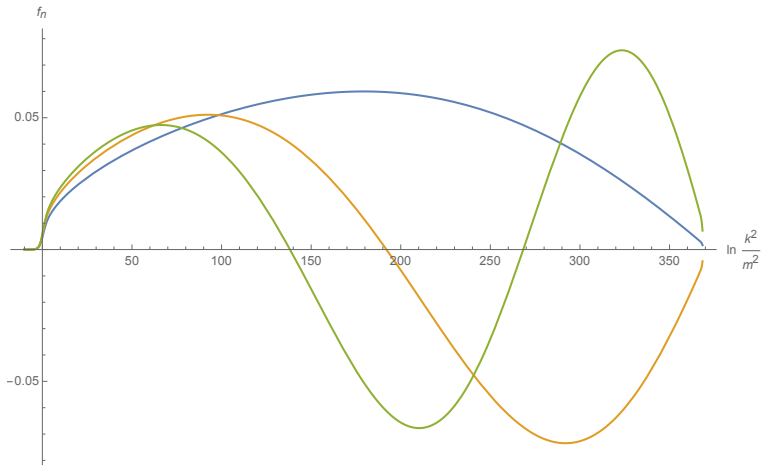

Figure 10. Behavior of the wave functions for a larger lattice limit $e^{t_{\max}} = e^{160}$.

For the slope, we extend our numerical analysis, keeping $N_{\text{step}} = 600$ fixed. Comparing $(e^{t_{\min}}, e^{t_{\max}}) = (10^{-40}, 10^{80})$ and $(e^{t_{\min}}, e^{t_{\max}}) = (10^{-40}, 10^{160})$

$$\begin{aligned} \alpha_1' &= 1.26 \times 10^{-5}\,, \qquad \alpha_1' = 3.17 \times 10^{-6} \\ \alpha_2' &= 1.77 \times 10^{-5}\,, \qquad \alpha_2' = 4.41 \times 10^{-6} \end{aligned} \tag{3.30}$$

we find analogous results also for the slope: they decrease with increasing lattice size.

Similarly, for the wave functions (see figure 10) with n-nodes we find that with increasing lattice size the nodes move into the UV region. i.e. the location of the extrema become larger with increasing lattice extension.

JHEP04(2020)183

As to numerical values of the radii of the leading state, we again compare $(e^{t_{\min}}, e^{t_{\max}}) = (10^{-40}, 10^{80})$ and $(e^{t_{\min}}, e^{t_{\max}}) = (10^{-40}, 10^{160})$:

$$< \ln \frac{k^2}{m^2} > = 88, \qquad < \ln \frac{k^2}{m^2} > = 174.83$$
$$r_1 = 6.8 \times 10^{18}\,\text{GeV}, \qquad r_1 = 4.98 \times 10^{37}\text{GeV}. \tag{3.31}$$

All these results further support our conclusion that, at $q^2 = 0$, our lattice formulation approximates the cut structure beginning at $E = 0$ with wave functions extending to very large momenta or even to infinity. We see that lattice artifacts are under control.

4 Summary and outlook

In this paper we have extended our previous analysis of the BFKL Pomeron to the Odderon case. We have performed a numerical analysis of the BFKL equation for conformal spin=1, using a massive infrared regulator and the running coupling constant, introduced with a specific prescription. The main result of our work is that the spectrum remains essentially the same as it was without cutoff and with fixed coupling. Let us note that in a forthcoming publication [31], M. Braun and G.P. Vacca have obtained very similar results: in that analysis a different infrared regulator is used which preserves the bootstrap condition of the BFKL equation. This supports the expectation that, in fact, the energy spectrum is fairly independent of the detailed form of the infrared regulator.

It is important to stress the differences between the QCD Odderon and the Pomeron. As already stated in the introduction, the same procedure applied to the BFKL Pomeron equation leads to a discrete set of Pomeron states with intercepts above one and nonvanishing t-slopes. Moreover, the leading state is soft and its wavefunction has its support in the region of small transverse momenta. In contrast, the Odderon has no such discrete states for the leading (BLV) family of solutions: the fixed cut starts at $\omega = 0$, the wave functions have very small slopes, and their main support lies in the UV region. To study the implications of this UV dominance one has to couple the rapidity dependent Odderon Green's function to specific external particle impact factors which have their characteristic hadronic scale. Because of the difference of the momentum scales one would expect that this coupling is small, at least much smaller than that of the leading Pomeron state.

It may be interesting to say a few words about the connection between the results of the present paper with the fixed point analysis performed in [26] in the soft region. In that paper we have investigated the interaction of Pomeron and Odderon fields, assuming that, away from the infrared region, we have non-vanishing self-interactions of the Pomeron and interactions of Pomeron and Odderon, in particular a (real valued) Pomeron $\to$ 2 Odderon vertex and an (imaginary) Odderon $\to$ Odderon+Pomeron vertex. We have found an infrared fixed point with two relevant (i.e. UV stable) directions. At this fixed point, both the Pomeron and the Odderon have intercept one and non vanishing slopes; the Odderon slope is slightly smaller than the Pomeron slope. When approaching this fixed point, in the parameter space of masses and interactions, from the IR stable directions both intercepts initially are above one, and in the IR limit they then approach unity, the Odderon slightly

JHEP04(2020)183

faster than the Pomeron. If we associate the IR momentum cutoff k with the radius R of the scattering system $k^2 \sim 1/R^2$, and assume $R^2 = R_0^2 + 2\alpha' \ln s$, we would expect that at large but finite energies the Odderon intercept would be slightly above unity, but smaller than the Pomeron intercept.

When trying to connect these results with the findings of the present paper, one would be tempted to draw the following picture. Starting in the UV region with the perturbative results for the Pomeron obtained in [24] and for the Odderon described in the present paper, one introduces interactions between Pomeron and Odderon fields and studies the RG flow as a function of the IR cutoff parameter k. In order to arrive at the IR fixed point described before, these interactions have to lower the initial intercept above one of the BFKL Pomeron field, but also to modify the fixed-cut structure of the Odderon state. A study of this transition is in progress.

Acknowledgments

J.B. expresses his gratitude for support and hospitality of the Departamento de Fisica, Universidad Tecnica Federico Santa Maria, Valparaiso, Chile and for the support of the INFN and the hospitality of the Bologna University. C.C. thanks for the financial support from the grant FONDECYT 1191434 and 1180118, Chile.

References

[1] TOTEM collaboration, *First determination of the ρ parameter at $\sqrt{s} = 13$ TeV: probing the existence of a colourless C-odd three-gluon compound state*, *Eur. Phys. J.* **C 79** (2019) 785 [arXiv:1812.04732] [INSPIRE].

[2] TOTEM collaboration, *First measurement of elastic, inelastic and total cross-section at $\sqrt{s} = 13$ TeV by TOTEM and overview of cross-section data at LHC energies*, *Eur. Phys. J.* **C 79** (2019) 103 [arXiv:1712.06153] [INSPIRE].

[3] TOTEM collaboration, *Recent Results from the CERN LHC Experiment TOTEM — Implications for Odderon Exchange*, *EPJ Web Conf.* **206** (2019) 06004 [arXiv:1903.06992] [INSPIRE].

[4] E. Martynov and B. Nicolescu, *Did TOTEM experiment discover the Odderon?*, *Phys. Lett.* **B 778** (2018) 414 [arXiv:1711.03288] [INSPIRE].

[5] L. Lukaszuk and B. Nicolescu, *A Possible interpretation of p p rising total cross-sections*, *Lett. Nuovo Cim.* **8** (1973) 405 [INSPIRE].

[6] A. Donnachie and P.V. Landshoff, *Multi-Gluon Exchange in pp Elastic Scattering*, *Phys. Lett.* **123B** (1983) 345 [INSPIRE].

[7] L.N. Lipatov, *Reggeization of the Vector Meson and the Vacuum Singularity in Nonabelian Gauge Theories*, *Sov. J. Nucl. Phys.* **23** (1976) 338 [INSPIRE].

JHEP04(2020)183

[8] E.A. Kuraev, L.N. Lipatov and V.S. Fadin, *Multi-Reggeon Processes in the Yang-Mills Theory*, *Sov. Phys. JETP* **44** (1976) 443 [INSPIRE].

[9] E.A. Kuraev, L.N. Lipatov and V.S. Fadin, *The Pomeranchuk Singularity in Nonabelian Gauge Theories*, *Sov. Phys. JETP* **45** (1977) 199 [INSPIRE].

[10] I.I. Balitsky and L.N. Lipatov, *The Pomeranchuk Singularity in Quantum Chromodynamics*, *Sov. J. Nucl. Phys.* **28** (1978) 822 [INSPIRE].

[11] J. Bartels, *High-Energy Behavior in a Nonabelian Gauge Theory (II). First Corrections to $T_{n\to m}$ Beyond the Leading In s Approximation*, *Nucl. Phys.* **B 175** (1980) 365 [INSPIRE].

[12] J. Kwiecinski and M. Praszalowicz, *Three Gluon Integral Equation and Odd c Singlet Regge Singularities in QCD*, *Phys. Lett.* **94B** (1980) 413 [INSPIRE].

[13] R.A. Janik and J. Wosiek, *Solution of the odderon problem*, *Phys. Rev. Lett.* **82** (1999) 1092 [hep-th/9802100] [INSPIRE].

[14] J. Bartels, L.N. Lipatov and G.P. Vacca, *A New odderon solution in perturbative QCD*, *Phys. Lett.* **B 477** (2000) 178 [hep-ph/9912423] [INSPIRE].

[15] J. Bartels, M.A. Braun, D. Colferai and G.P. Vacca, *Diffractive eta(c) photoproduction and electroproduction with the perturbative QCD odderon*, *Eur. Phys. J.* **C 20** (2001) 323 [hep-ph/0102221] [INSPIRE].

[16] C. Ewerz, *The Odderon in quantum chromodynamics*, hep-ph/0306137 [INSPIRE].

[17] M. Braun, G.P. Vacca and G. Venturi, *Properties of the hard Pomeron with a running coupling constant and the high-energy scattering*, *Phys. Lett.* **B 388** (1996) 823 [hep-ph/9605304] [INSPIRE].

[18] H. Kowalski, L.N. Lipatov, D.A. Ross and O. Schulz, *Decoupling of the leading contribution in the discrete BFKL Analysis of High-Precision HERA Data*, *Eur. Phys. J.* **C 77** (2017) 777 [arXiv:1707.01460] [INSPIRE].

[19] H. Kowalski, L.N. Lipatov and D.A. Ross, *The Behaviour of the Green Function for the BFKL Pomeron with Running Coupling*, *Eur. Phys. J.* **C 76** (2016) 23 [arXiv:1508.05744] [INSPIRE].

[20] H. Kowalski, L. Lipatov and D. Ross, *The Green Function for the BFKL Pomeron and the Transition to DGLAP Evolution*, *Eur. Phys. J.* **C 74** (2014) 2919 [arXiv:1401.6298] [INSPIRE].

[21] E. Levin, L. Lipatov and M. Siddikov, *BFKL Pomeron with massive gluons*, *Phys. Rev.* **D 89** (2014) 074002 [arXiv:1401.4671] [INSPIRE].

[22] E. Levin, L. Lipatov and M. Siddikov, *Semiclassical solution to the BFKL equation with massive gluons*, *Eur. Phys. J.* **C 75** (2015) 558 [arXiv:1508.04118] [INSPIRE].

[23] E. Levin, L. Lipatov and M. Siddikov, *BFKL Pomeron with massive gluons and running coupling*, *Phys. Rev.* **D 94** (2016) 096004 [arXiv:1608.03816] [INSPIRE].

[24] J. Bartels, C. Contreras and G.P. Vacca, *A functional RG approach for the BFKL Pomeron*, *JHEP* **01** (2019) 004 [arXiv:1808.07517] [INSPIRE].

[25] J. Bartels, C. Contreras and G.P. Vacca, *Could reggeon field theory be an effective theory for QCD in the Regge limit?*, *JHEP* **03** (2016) 201 [arXiv:1512.07182] [INSPIRE].

[26] J. Bartels, C. Contreras and G.P. Vacca, *Pomeron-Odderon interactions in a reggeon field theory*, *Phys. Rev.* **D 95** (2017) 014013 [arXiv:1608.08836] [INSPIRE].

JHEP04(2020)183

[27] M. Ciafaloni, D. Colferai and G.P. Salam, *Renormalization group improved small x equation*, *Phys. Rev.* **D 60** (1999) 114036 [hep-ph/9905566] [INSPIRE].

[28] A. Sabio Vera, *An 'All-poles' approximation to collinear resummations in the Regge limit of perturbative QCD*, *Nucl. Phys.* **B 722** (2005) 65 [hep-ph/0505128] [INSPIRE].

[29] J. Bartels, V.S. Fadin, L.N. Lipatov and G.P. Vacca, *NLO Corrections to the kernel of the BKP-equations*, *Nucl. Phys.* **B 867** (2013) 827 [arXiv:1210.0797] [INSPIRE].

[30] J. Bartels and G.P. Vacca, *Generalized Bootstrap Equations and possible implications for the NLO Odderon*, *Eur. Phys. J.* **C 73** (2013) 2602 [arXiv:1307.3985] [INSPIRE].

[31] M.A. Braun and G.P. Vacca, *The odderon and BKP states in the Quantum Chromodynamics*, arXiv:2001.05199 [INSPIRE].

JHEP04(2020)183